33rd Annual International Conference of the IEEE EMBS
Boston, Massachusetts USA, August 30 - September 3, 2011

Integrating Active Shape Models into Ultrasound Elastography to Diagnose Musculoskeletal Injuries: a 2D Simulation Study

Amy L. Cochran and Yingxin Gao

***Abstract*-We build on ultrasound elastography (UE) by offering a new method for diagnosing musculoskeletal injuries from estimated tissue displacements. Our strategy is to isolate the portion of tissue displacements that arise due to injury. Active shape models are constructed capturing displacement variation among normal tissue. New tissue is then evaluated by estimating displacements with (1) the active shape models and (2) a traditional UE tracking algorithm. The difference between the two estimates defined *virtual axial displacement* and used to identify injured tissue. Our method was tested by simulating planar tissue examined with ultrasound elastography. Images are presented of axial displacement and virtual axial displacement as well as axial strain and *virtual axial strain,* i.e. partial derivative of the respective displacements with respect to the axial coordinate. Injured tissue and uninjured tissue were not statistically different when comparing mean absolute value of axial strain covarying with the loading conditions. In contrast, uninjured tissue and injured tissue were statistically different when comparing absolute value of virtual axial strain covarying with loading conditions ($p < 0.0001$). Statistical significance was considered $p < 0.05$.**

I. Introduction

ULTRASOUND elastography (UE) is a promising tool for evaluating mechanical behavior of soft tissue [1]. Originally developed as an alternative to palpation, UE has been used to diagnose pathologies such as cancer and liver cirrhosis [2]. Recent work has focused on developing UE techniques to diagnose musculoskeletal soft tissue injuries [3]–[7]. Although there are several approaches to UE, one particular paradigm is to estimate strain during quasi-static loading. The goal of quasi-static UE is to identify pathology from estimated strain.

When identifying musculoskeletal injury from strain, it is possible either to solve inversely for material properties or use strain as a qualitative measure of stiffness. Each approach is based on simplifying assumptions about material behavior such as linearity, uniform stress, isotropy, and plane strain [1],[2],[8],[9]. In contrast, musculoskeletal soft tissue is nonlinear and anisotropic [10]. Although these assumptions are inaccurate, even a poor estimate of Young's modulus—or analogously tangent moduli for nonlinear materials—may contain good diagnostic information. Therefore, the key question is not whether a strain analysis provides accurate material properties, but whether a strain analysis can resolve an injury. This question motivates our interest in strain analyses that are not based on estimating material properties.

Our goal is to isolate the portion of tissue displacements that arise due to injury. To this end, uninjured tissue is used to construct active shape models [11], statistical models that capture image variations within a specific problem. In our problem, these models are used to capture displacement variations among uninjured tissue. Sources of variation include changes in loading, imaging, geometry, and native mechanical properties. New tissue is then evaluated by estimating displacements with two methods: 1) the active shape models and 2) traditional UE techniques. Diagnoses are made using the difference between the two estimates, which we call *virtual axial displacement*.

In this paper, we take a first look at our strategy. We proceed by describing our method and simulation of events in which injured and uninjured planar tissues are examined with ultrasound elastography. The events were represented by a probability model that reflected in vivo statistical variation. We conclude by discussing our results.

II. Method

A. Background

We restrict our attention to 2D ultrasound and axial displacements—i.e. displacements along the direction of wave propagation. Let axial displacements be denoted by a function $u : \mathbb{R}^2 \to \mathbb{R}$. If a set V contains *all possible* functions of axial displacements that could occur were the tissue of interest uninjured, then our goal is resolve differences between u and every $v \in V$. By definition, V incorporates variations in displacements that arise when examining tissue.

To improve contrast between injured and uninjured tissue, we subtract from u the function $\bar{v} \in V$ most "similar" to u:

$$w \equiv u - \bar{v}, \tag{1}$$

$$\bar{v} \equiv argmax\{g(u,v): v \in V\}. \tag{2}$$

Here, g is some function that measures "similarity" between u and v. For uninjured tissue, u lies in V, and so, $w = 0$. Consequently, for injured tissue, w is compared to zero, which leads to perfect contrast provided that $u \notin V$. The function w is called *virtual axial displacement*. In practice, V, u, and $\bar{v}$ are estimated. Active shape models and traditional UE algorithms allow for these estimations.

B. Active shape models

To estimate the set V, a training set is constructed by applying quasi-static loading to m uninjured musculoskeletal structures and calculating displacements. With 2D ultrasound, displacements are calculated in the axial and lateral directions. (The lateral direction is perpendicular to the axial.) Displacements are measured on an $(n+1) \times$

Manuscript received March 26, 2011. This work was supported by the Sibley School of Mechanical and Aerospace Engineering at Cornell University.

A.L. Cochran is with the Center for Applied Mathematics, Cornell University, Ithaca, NY 14853 USA (phone: 603-686-1489; e-mail: alc98@cornell.edu).

Y. Gao is with the Sibley School of Mechanical and Aerospace Engineering and the Center for Applied Mathematics, Cornell University, Ithaca, NY 14853 USA (e-mail: yg75@cornell.edu).

$(p+1)$ grid, in which points are spaced at intervals of equal *fractional* distance along and transverse to the structure. An axial displacement image and its corresponding lateral displacement image are together reshaped into a $2(n+1)(p+1)\times 1$ vector, which designates a column of a matrix X. Eigenvectors and eigenvalues are calculated for the covariance matrix $(X-\mu)(X-\mu)^T$, where μ is the column mean of X. The vector μ is transformed back into mean axial and lateral images, ζ and ξ; the eigenvectors are transformed back into axial and lateral eigenimages, A_i and L_i. A subset of k axial and lateral eigenimages, $\{A_i, L_i\}_{i=1}^{k}$, and their corresponding eigenvalues, $\{\lambda_i\}_{i=1}^{k}$, are kept for subsequent analysis. Constructed images estimate V:

$$V \approx \left\{\zeta + \textstyle\sum_{i=1}^{k} a_i\, A_i :\ a \in \mathbb{R}^k\right\}. \quad (3)$$

C. Displacement estimation

Displacement functions, u and $\bar{v}$ are estimated for new tissue using active shape models and traditional UE methods. The tissue of interest is deformed, ultrasound images are captured, and the grid of $(n+1)\times(p+1)$ points is defined. Let r and c be matrices that contain axial and lateral coordinates of these points, and I_0 and I_1 denote ultrasound images captured before and after deformation. First, $\bar{v}$ is estimated by finding $a \in \mathbb{R}^k$ that maximizes:

$$f(\, I_0(r,c),\, I_2(a)), \quad (4)$$

where

$$I_2(a) \coloneqq I_1\big(r + \zeta + \textstyle\sum_{i=1}^{k} a_i A_i\,, c + \xi + \sum_{i=1}^{k} a_i L_i\big). \quad (5)$$

The function f measures similarity between two ultrasound images. Notice f is related to g at (2). The maximizer at (4), $\tilde{a} \in \mathbb{R}^k$, gives

$$\bar{v} = \zeta + \textstyle\sum_{i=1}^{k} \tilde{a}_i A_i. \quad (6)$$

Next, displacements are estimated using UE displacement estimation. To improve computational efficiency, the displacements are initially seeded with:

$$\zeta + \textstyle\sum_{i=1}^{k} \tilde{a}_i A_i\,;\ \xi + \sum_{i=1}^{k} \tilde{a}_i L_i. \quad (7)$$

The function u is given by the resulting axial displacement estimations. Injuries are diagnocx`sed by comparing virtual axial displacements, $w = u - \bar{v}$, among different tissues.

III. Simulation

A. Training

A probability model simulated events that uninjured musculoskeletal tissue was uniaxially stretched while being imaged with ultrasound. Geometry, material behavior, imaging window, and loading were represented by thirteen parameters, each of which was as a uniform random variable (Table 1). Geometry was designed to resemble a planar view of a ligament along its long axis (Fig. 1). Material behavior

TABLE I
Simulation Parameters

Symbol	Quantity	Range
H	Tissue height	5–10 mm
T	Width to height ratio	3–4
α	Quadratic coefficient	0-0.025
R_1, R_2	Radii	6–9 mm
A_1	Location parameter	$¾\sqrt{R_1^2-h^2}$–$\sqrt{R_1^2-h^2}$
A_2	Location parameter	$¾\sqrt{R_2^2-h^2}$–$\sqrt{R_2^2-h^2}$
C_1, C_2	Material constants	5–15 MPa
C_3	Material constant	50-250 MPa
ε	Material constant	500-1500 MPa
S	Global stretch	0.01–0.04
θ	Imaging angle	-5–5°
L_1, L_2	Damage location	Within the tissue
R_3	Radius of damage region	1–5 mm

Parameters represented events that musculoskeletal tissue is loaded quasi-statically while imaged with ultrasound.

was expressed by a nearly incompressible, transversely isotropic strain energy function for fibrous soft tissue [10]:

$$C_1(\bar{I}_1-3) + C_2(\bar{I}_2-3) + C_3\left(\mathrm{e}^{\bar{I}_4-1} - \bar{I}_4\right) + \frac{\varepsilon}{2}\ln(J)^2, \quad (8)$$

where $\bar{I}_1$, $\bar{I}_2$, and $\bar{I}_4$ are invariants of the isochoric portion of the right Cauchy-Green tensor and J is the determinant of the deformation tensor. The constants, C_1, C_2, C_3, and ε were random variables, and fiber direction varied linearly between surface tangents. Imaging window was specified by θ, the angle between the axial direction and the tissue's short axis. Tissues were stretched by a factor S.

A set of 85 vectors of thirteen parameters were randomly sampled. Regions were meshed using triangular elements [13], and, assuming plane strain, Finite Element Analysis (FEA) estimated tissue displacements during events represented by the sampled vectors. Tissue displacements were resampled on a 501×501 grid defined using fractional distance. Eigenimages were constructed and a subset was kept explaining 99.999% of the variation.

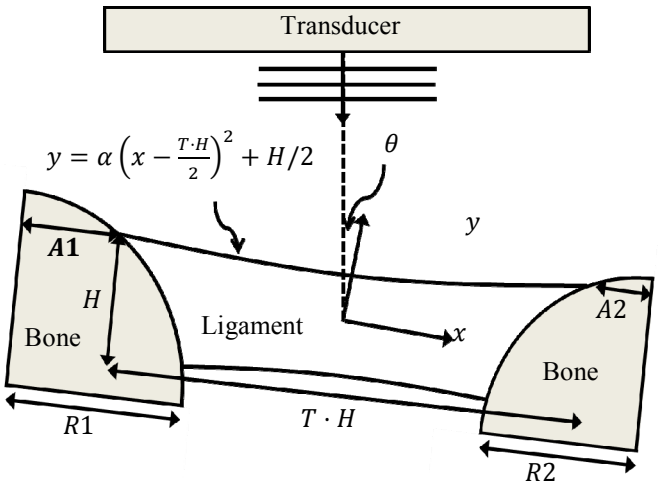

Fig. 1: Tissue geometry resembled a ligament-bone complex along its long axis. Imaging window was specified by an angle θ.

B. Displacement Estimation

Displacements were estimated for simulated uninjured and injured tissue structures examined with ultrasound during

uniaxial loading. Uninjured tissue was modeled using the previously described parameters. Injured tissue was modeled similarly except an additional parameter, D, was incorporated into the isochoric portion of strain energy [14]:

$$(1-D)\left(C_1(\bar{I}_1-3)+C_2(\bar{I}_2-3)+C_3\left(e^{\bar{I}_4-1}-\bar{I}_4\right)\right). \quad (9)$$

The parameter D represented fractional damage of matrix and fibers. Damage was restricted to a circular region. Three uniform random variables designated the region's location and radius, and D was set to 0.50 at the center and decreased quadratically to zero at the edge of the region.

Two sets of 20 random vectors were sampled. One set represented uninjured tissue, and the other set represented injured tissue. Each vector had the original thirteen parameters, whereas vectors in the injured set contained the additional three damage parameters. FEA was again used to calculate displacements. With the displacements, Field II software [15],[16] simulated ultrasound images captured before and after deformation. A 7MHz linear transducer with 192 elements was used. Sampling frequency was 100 MHz and A-line spacing was 0.176 mm. Ultrasound images were up-sampled laterally by a factor of 8.

Displacements were estimated from the ultrasound images using the active shape models and the quality-guided method [17] as the traditional UE algorithm. Normalized cross-correlation was used for the function f at (2), whereas MATLAB's *fmincon* solved for the maximizer $\tilde{a}$. The values a_i were constrained to lie between $-3\sqrt{\lambda_i}$ to $3\sqrt{\lambda_i}$. Axial by lateral size of the window was 2.20 mm by 2.20 mm; window overlap was 97% and 90% in axial and lateral directions respectively. Displacements were smoothed using denoising [18],[19], median [20], and low pass filters.

C. Statistical Analysis

Linear least squares [21] was used to estimate axial strain and *virtual axial strain*, partial derivatives of u and w with respect to the axial coordinate. Mean absolute value of each strain was calculated over the entire structure. Linear regressions were fit for each mean and loading conditions T. Regression were compared using Analysis of Covariance, which entails testing for statistical differences between slopes, and, when the slopes are not different, testing for differences between y-intercepts. Multivariate linear regressions were fit by including fractional area of damage region as a dependent variable. P-values were calculated using Student's t-test and significance was $p < 0.05$.

IV. Results

Twelve eigenvectors explained 99.999% of the variance in displacements, despite varying imaging window, material properties, geometry, and loading. The dominant eigenvector alone captured 98% of the variance. Images of virtual axial displacement illustrate that axial displacements in injured tissue deviated from those in normal tissue around the injury (Fig. 2). In the strain images, injuries were located for more negative values in axial strain and virtual axial strain. Edges effects were present in both types of strain images.

Mean absolute axial strain and mean absolute virtual axial strain covaried linearly with the loading conditions. Mean absolute axial strain and the loading conditions had a strong linear relationship for both uninjured ($R^2 = 0.97$) and injured tissue ($R^2 = 0.97$) (Fig. 3). Comparitively, mean absolute virtual axial strain and the loading conditions had a weaker linear relationship for uninjured ($R^2 = 0.84$) and injured tissue ($R^2 = 0.74$) (Fig. 4). The regression lines indicate that the accuracy of the active shape models deteriorated with increasing loading conditions.

Mean absolute virtual axial strain was a better indicator of injury than mean absolute axial strain. The images showed that axial strain was more negative in the injured region, but slopes of the lines for mean absolute axial strain were not statistically different ($p = 0.10$). Assuming equal slopes, the y-intercepts were not statistically different ($p = 0.13$). In contrast, slopes of the lines for mean absolute virtual strain were statistically different ($p < .0001$). When fractional area of damage was included in the linear regression, the coefficient of this variable was not statistically significant for modeling mean absolute axial strain ($p = 0.52$), but was statistically significant and postive for modeling mean absolute virtual axial strain ($p < 0.0001$). By including fractional area of damage, 90% of the variance in mean absolute virtual axial strain was explained.

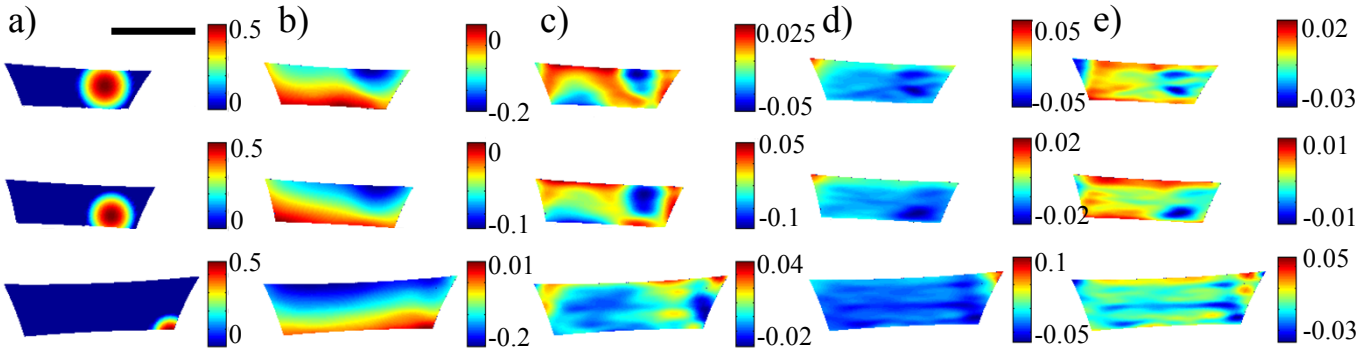

Fig. 2: Images of injured tissues show a) damage, b) axial displacement (mm), c) virtual axial displacement (mm), d) axial strain, and e) virtual axial strain. Virtual axial displacements deviated from zero around the damage region, and axial strain and virtual axial strain were more negative in the damage region. Scale bar represents 10 mm.

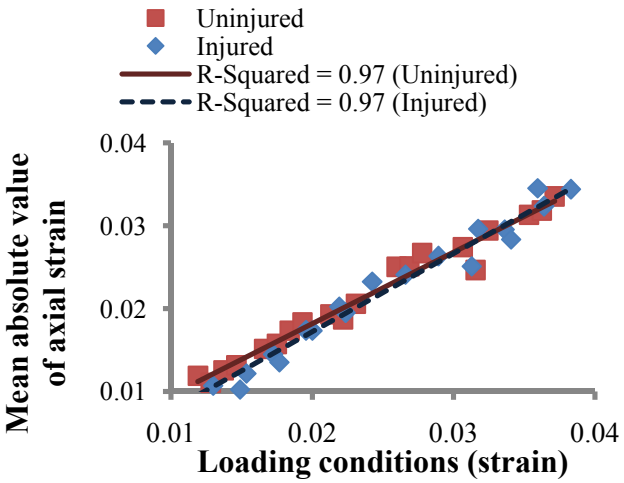

Fig. 3: Mean absolute value of axial strain was linearly related to the loading conditions. The slopes of the two lines were not statistically different, and, assuming equal slopes, the y-intercepts were not statistically different.

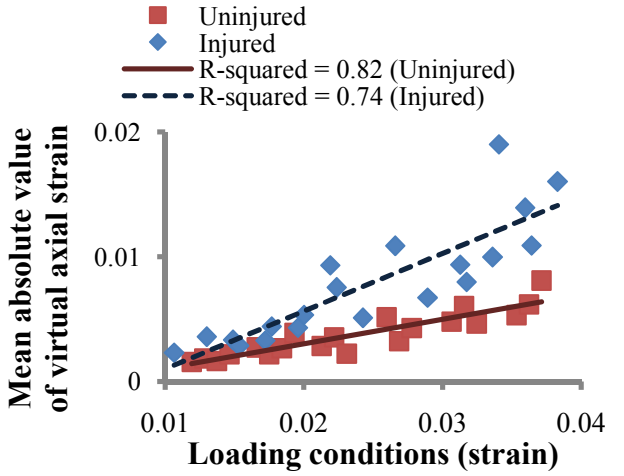

Fig. 4: Mean absolute value of virtual axial strain was linearly related to the loading conditions. The slopes of the two lines were statistically different ($p < 0.0001$).

V. Discussion

We proposed a method to diagnose musculoskeletal injuries that combines techniques from active shape models and ultrasound elastography. Our method was tested by simulating events in which injured and uninjured musculoskeletal tissues were deformed while imaged with ultrasound. A probability model incorporated statistical variation, which arises among patients and examinations. Our results indicate that by isolating displacements that arise due to an injury, we can increase statistical differences between uninjured and injured tissues.

Due to promising results, future work will continue to improve on our method and compare it to current approaches in more realistic scenarios. Our study required only a small number of eigenimages, but it is expected that more will be needed to capture the same variance in more realistic tissue. Computational efficiency will also be explored to determine whether real-time feedback can be achieved. In the worst case scenario, our method would require the time it takes to run each tracking algorithm individually, but we expect much better performance, since displacements are seeded in the second algorithm. Lastly, a possible extension is to use active appearance models [22], a variant of active shape models that would include variation in ultrasound images.

References

[1] J. Ophir, I. Cespedes, H. Ponnekanti, Y. Yazdi, X. Li, "Elastography: A quantitative method for imaging the elasticity of biological tissues," *Ultrasonic Imaging*, vol. 13, pp. 111-34, Apr. 1991.

[2] J. Ophir et al., "Elastography: imaging the elastic properties of soft tissues with ultrasound," *J Med Ultrasonics*, vol. 29, pp. 155–171, 2002.

[3] P.L. Kuo, P.C. Li, C.T. Shun and J.S. Lai, "Strain measurements of rabbit Achilles tendons by ultrasound," *Ultrasound Med Biol*, vol. 25, pp. 1241–1250, 1999.

[4] E.E. Drakonaki, G.M. Allen, and D.J. Wilson, "Real-time ultrasound elastography of the normal Achilles tendon: reproducibility and pattern description," *Clinical Radiology*, vol. 64, Dec. 2009.

[5] T. De Zordo, et al., "Real-time sonoelastography of lateral epicondylitis: comparison of findings between patients and healthy volunteers," *AJR Am J Roentgenol*, vol. 193, pp. 180–185, 2009.

[6] T. De Zordo, et al., "Real-time sonoelastography findings in healthy Achilles tendons," *AJR Am J Roentgenol*, vol. 193:W134–38, 2009.

[7] A. Kapoor et al., "Realtime elastography in plantar fasciitis: comparison with ultrasonography and MRI," *Current Orthopedic Practice*, vol. 21, pp. 600-608, Nov/Dec 2010.

[8] P. Barbone, and J. Bamber, "Quantitative elasticity imaging: what can and cannot be inferred from strain images," *Phys Med Biol*, vol. 47, 2147–2164, 2002.

[9] M.M. Doyley, S. Srinivasan, S.A. Pendergrass, Z. Wu, and J. Ophir, "Comparative evaluation of strain-based and model-based modulus elastography," *Ultra Med Bio*, vol. 31, pp. 787-802, June 2005.

[10] J.A. Weiss, B.N. Maker, S. Govindjee, "Finite element implementation of incompressible, transversely isotropic hyperelasticity," *Comput Meth Appl Mech Eng*, vol. 135, pp. 107-28, 1996.

[11] T.F. Cootes, C.J. Taylor, D.H. Cooper, and J. Graham, "Active shape models—Their training and application," *Comput Vis Image Und*, vol. 61, pp.38-59, 1995.

[12] J.G. Bosch, et al., "Computer-aided diagnosis via model-based shape analysis: Automated classification of wall motion abnormalities in echocardiograms," *Acad Radiol*, vol. 12, pp. 358-367, Mar. 2005.

[13] P-O. Persson, G. Strang, "A Simple Mesh Generator in MATLAB," *SIAM Review*, vol. 46, pp. 329-345, June 2004.

[14] B. Calvo, E. Peña, M.A. Martinez, M. Doblaré, "An uncoupled directional damage model for fibred biological soft tissues. Formulation and computational aspects," *Int J Numer Meth Engng*, vol. 69, pp. 2036-2057, 2007.

[15] J.A. Jensen. "Field: A Program for Simulating Ultrasound Systems," *Paper presented at the 10th Nordic-Baltic Conference on Biomedical Imaging Published in Med Biol Eng Comput*, vol. 34pp. 351-353, 1996.

[16] J.A. Jensen, N.B. Svendsen, "Calculation of pressure fields from arbitrarily shaped, apodized, and excited ultrasound transducers," *IEEE Trans Ultrason Ferroelec Freq Cont*, vol. 39, pp. 262-67, 1992.

[17] L. Chen, G.M. Treece, J.E. Lindop, A.H. Gee, R.W. Prager, "A quality-guided displacement tracking algorithm for ultrasonic elasticity imaging," *Med Image Anal*, vol. 13, pp. 286–296, 2009.

[18] A. Chambolle, "An algorithm for total variation minimization and applications," *J Math Imaging Vis*, vol. 20, pp. 89–97, 2004.

[19] X. Bresson, T. Chan, "Fast dual minimization of the vectorial total variation norm and applications to color image processing," *CAM Report 07-25*, 2007.

[20] M.M Doyley, J.C. Bamber, F. Fuechsel, and N.L. Bush, "A freehand elastographic imaging approach for clinical breast imaging: system development and performance evaluation," *Ultrasound Med Biol*, vol. 10, pp. 1347-1357, 2001.

[21] F. Kallel, J. Ophir, "A least-squares strain estimator for elastography," *Ultrasonic Imaging*, vol. 19, pp. 195–208, 1997.

[22] T.F Cootes, G.J. Edwards, C.J. Taylor, "Active appearance models," *IEEE Trans Pattern Anal Mach Intell*, vol.23, pp.681-85, Jun 2001.